REGULAR PAPERS

Robust analysis method for acoustic properties of biological specimens measured by acoustic microscopy

Japanese Journal of Applied Physics **57**, 07LB07 (2018)
https://doi.org/10.7567/JJAP.57.07LB07

REGULAR PAPER

Robust analysis method for acoustic properties of biological specimens measured by acoustic microscopy

Mototaka Arakawa[1,2*], Shohei Mori[2], Hiroshi Kanai[2,1], Ryo Nagaoka[1], Miki Horie[1], Kazuto Kobayashi[3], and Yoshifumi Saijo[1]

[1]*Graduate School of Biomedical Engineering, Tohoku University, Sendai 980-8579, Japan*
[2]*Graduate School of Engineering, Tohoku University, Sendai 980-8579, Japan*
[3]*Department of Research and Development, Honda Electronics Co., Ltd., Toyohashi, Aichi 441-3193, Japan*

*E-mail: arakawa@ecei.tohoku.ac.jp

Received November 6, 2017; revised December 30, 2017; accepted January 2, 2018; published online April 20, 2018

We proposed a robust analysis method for the acoustic properties of biological specimens measured by acoustic microscopy. Reflected pulse signals from the substrate and specimen were converted into frequency domains to obtain sound speed and thickness. To obtain the average acoustic properties of the specimen, parabolic approximation was performed to determine the frequency at which the amplitude of the normalized spectrum became maximum or minimum, considering the sound speed and thickness of the specimens and the operating frequency of the ultrasonic device used. The proposed method was demonstrated for a specimen of malignant melanoma of the skin by using acoustic microscopy attaching a concave transducer with a center frequency of 80 MHz. The variations in sound speed and thickness analyzed by the proposed method were markedly smaller than those analyzed by the method based on an autoregressive model. The proposed method is useful for the analysis of the acoustic properties of bilogical tissues or cells.

1. Introduction

Acoustic microscopy[1–3] is one of the useful modalities for tissue characterization, because it can obtain acoustic properties, viz., sound speed and attenuation, in a microscopic region. Usually, thin-sliced specimens with a thickness of about 10 μm are used for measurements. It is impossible to separate the reflected signals from the front and back surfaces of a specimen if rf tone burst signals are used as input signals. To obtain the thickness and sound speed of the specimen, it is necessary to measure the frequency characteristics of the superposed signal as the interference output. However, it is time-consuming. Thus, pulse signals are widely used as input signals.[4]

Acoustic property measurement methods for biological specimens using pulse signals by acoustic microscopy were broadly divided into time and frequency domain analyses. In time domain analysis, the arrival times of reflected pulses from the substrate surface without a specimen and the front and back surfaces of the specimen are measured to obtain the sound speed and thickness. The pulse spectrum method is the analysis method in the frequency domain.[5] It is possible to obtain the thickness and sound speed of the specimen simultaneously from the amplitude and phase of the frequency spectrum of the reflected signals. In addition, a method using an autoregressive (AR) model was proposed[6,7] and the software was installed into a commercial acoustic microscopy system.[8]

Acoustic microscopy has been applied to the characterization of biological tissues and cells.[9–31] Water or physiological saline solution is used for the coupler in the measurements of biological specimens. Then, the reflected signal from the specimen surface, S_S, shown in Fig. 1 becomes small, because the acoustic impedance difference between the specimen and the coupler is small. The backscattered waves produced by the inhomogeneity inside biological specimens might be larger than the signal S_S. Thus, sound speed and thickness errors would be fairly large. In this paper, a robust analysis method for the acoustic properties of biological specimens measured by acoustic microscopy is discussed.

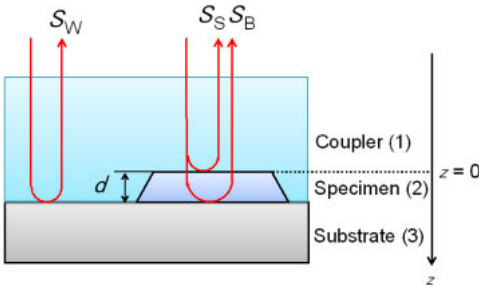

Fig. 1. (Color online) Measurement signals for acoustic property measurement by acoustic microscopy.

2. Analysis method

Figure 1 shows the measurement signals for the acoustic property measurements of biological specimens. Each specimen is placed on a substrate such as a slide glass or a petri dish. The ultrasonic waves emitted from the ultrasonic transducer were irradiated to the specimen through a coupler such as water or physiological saline solution. S_W, S_S, and S_B are the reflected signals from the substrate surface, the specimen surface, and the boundary between the specimen and the substrate, respectively. On the basis of the acoustic transmission line model, these signals are represented as

$$S_W = A \cdot R_{13} \cdot \exp(-2\gamma_1 d), \tag{1}$$

$$S_S = A \cdot R_{12}, \tag{2}$$

$$S_B = A \cdot T_{12} \cdot R_{23} \cdot T_{21} \cdot \exp(-2\gamma_2 d), \tag{3}$$

$$\gamma_i = \alpha_i + jk_i, \tag{4}$$

where A is the amplitude coefficient, R_{ij} and T_{ij} are the reflection and transmission coefficients from medium i to medium j, respectively, γ_i is the propagation constant, α_i is the attenuation coefficient, k_i is the wave number, and d is the thickness of the specimen. The coupler, specimen, and substrate are media 1, 2, and 3, respectively. If the signals S_S and S_B cannot be separated in the time domain, the superposed signal of S_S and S_B normalized by the signal S_W is expressed as

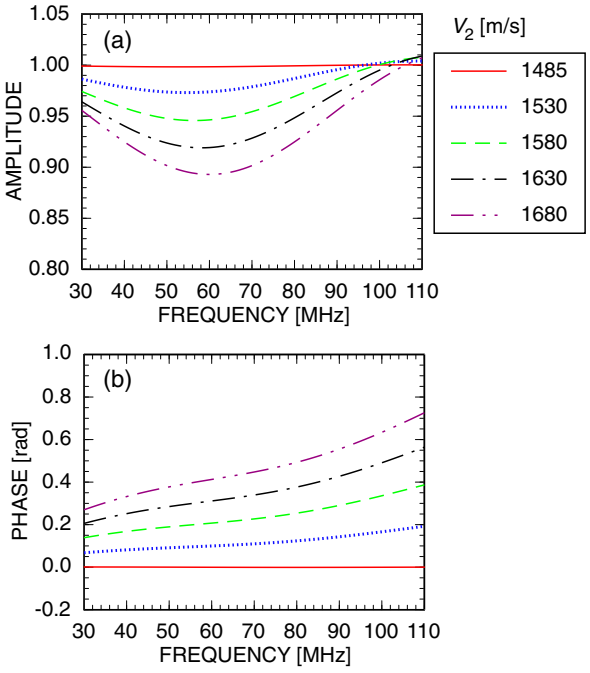

Fig. 2. (Color online) Frequency spectra of (a) amplitude and (b) phase calculated by changing V_2.

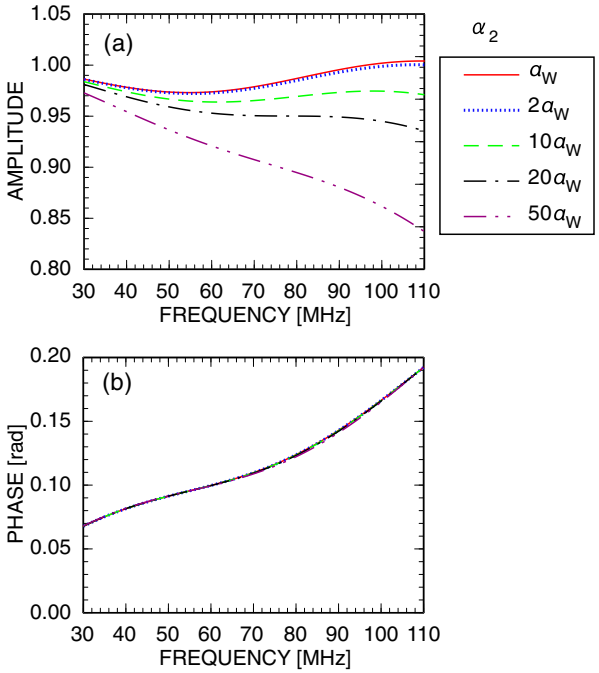

Fig. 3. (Color online) Frequency spectra of (a) amplitude and (b) phase calculated by changing α_2.

$$\frac{S_S + S_B}{S_W} = \frac{R_{12}}{R_{13}} \cdot \exp(2\gamma_1 d) \times \left[1 + \frac{T_{12} \cdot R_{23} \cdot T_{21}}{R_{12}} \cdot \exp(-2\gamma_2 d)\right]. \quad (5)$$

By performing Fourier transform for the signal, the frequency spectrum can be obtained. From the frequency f_m at which the amplitude spectrum becomes maximum or minimum and the phase ϕ_m of the phase spectrum at f_m, the thickness d and sound speed V_2 of the specimen were obtained from[5)]

$$d = \frac{V_1}{4\pi f_m}(\phi_m + n\pi), \quad (6)$$

$$V_2 = \left(\frac{1}{V_1} - \frac{\phi_m}{4\pi f_m d}\right)^{-1}, \quad (7)$$

where n is the natural number.

The following equation can be obtained by transforming Eq. (6):

$$\phi_m = \frac{4\pi f_m d}{V_1} - n\pi. \quad (8)$$

Equation (9) was obtained by substituting V_1 in Eq. (7) into Eq. (8).

$$V_2 = \frac{4 f_m d}{n}. \quad (9)$$

The amplitude and phase of the frequency spectra calculated using Eq. (5) by changing the sound speed of the specimen, V_2, are shown in Fig. 2. Here, water ($V_1 = 1485\,\mathrm{m/s}$, $\rho_1 = 998\,\mathrm{kg/m^3}$, $\alpha_1 = \alpha_W = 2.23 \times 10^{-14}\,\mathrm{s^2/m}$) was used as the coupler. The density and thickness of the specimen were assumed to be $1000\,\mathrm{kg/m^3}$ and $7\,\mu\mathrm{m}$, respectively. The attenuation coefficient of the specimen, α_2, was assumed to be equal to α_W. The amplitude of the interference of the amplitude spectrum increased with V_2, because the acoustic impedance difference between the specimen and water increased. Moreover, the rate of phase change increased with V_2. Next, the amplitude and phase of the frequency spectra were calculated by changing the attenuation coefficient of the specimen, α_2, when water was used as the coupler. The results are shown in Fig. 3. The sound speed, density, and thickness of the specimen were assumed to be $1530\,\mathrm{m/s}$, $1000\,\mathrm{kg/m^3}$, and $7\,\mu\mathrm{m}$, respectively. The amplitude of the interference of the amplitude spectrum decreased with increasing α_2. In particular, monotonic decreases in the amplitude spectrum were observed when α_2 was more than 20 times larger than α_W. Phase changes were almost the same regardless of α_2.

Relationships among ϕ_m, V_2, and f_m for each n can be obtained using Eqs. (8) and (9), if d is known. The relationship for $n = 1$, that is, the first minimum in the frequency spectrum, is shown in Fig. 4. f_m exists in the frequency range of 40–105 MHz if d is 4–8 μm and V_2 is 1,400–1,700 m/s. In the case of $n = 2$, f_m exists in the same frequency range if d is 8–16 μm from Eq. (9). Therefore, it is possible to predict the frequency range of the maxima and minima of the amplitude spectrum, if the thickness and sound speed of the specimen and the operating frequency range of the ultrasonic device used in the measurement are known. The frequency f_m might shift if there exist ripples on the amplitude spectrum produced by the scattered wave and multiple reflections. To reduce the effects and robustly obtain the average properties, f_m can be determined as follows.

(1) The frequency f_m at which the amplitude spectrum becomes maximum or minimum is calculated by the parabolic approximation of the amplitude spectrum considering the sound speed and thickness of the specimen and the operating frequency range of the ultrasonic device.

(2) d and V_2 are calculated using Eqs. (6) and (7) using f_m and ϕ_m.

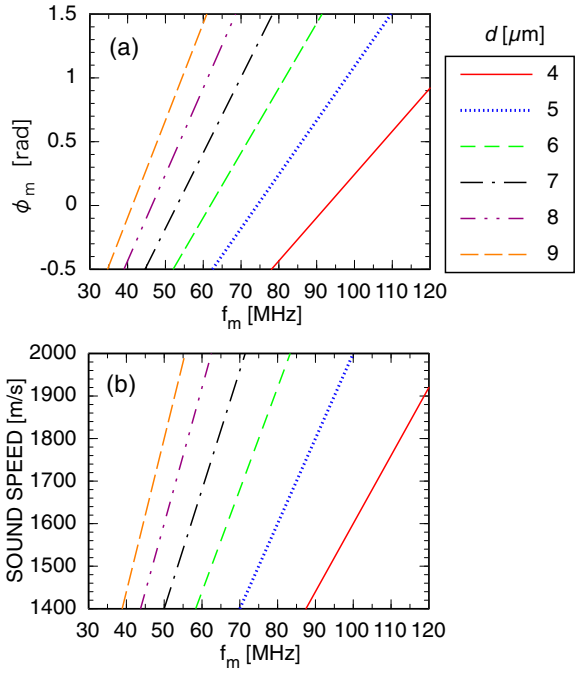

Fig. 4. (Color online) Relationships among phase of the phase spectrum, ϕ_m, sound speed of specimen, V_2, and frequency at which the amplitude spectrum becomes minimum, f_m. (a) ϕ_m vs f_m and (b) V_2 vs f_m.

Table I. Results analyzed by the proposed method for the amplitude and phase spectra in Fig. 2.

V_2 (m/s)	Analyzed results		
	f_m (MHz)	Thickness (μm)	Sound speed (m/s)
1485	53	7.005	1485.0
1530	55	6.955	1530.1
1580	56	7.052	1579.7
1630	58	7.025	1629.7
1680	60	7.000	1680.0

The average acoustic properties of the specimen will be obtained even if ripples exist on the amplitude spectrum, because the proposed method can obtain a single maximum or minimum point from the entire frequency range of the amplitude spectrum.

Sound speed and thickness were obtained by the proposed method for the frequency spectra in Figs. 2 and 3. Their results are shown in Tables I and II, respectively. The analyzed sound speed error was within 0.3 m/s for $\alpha_2 = \alpha_W$. On the other hand, the sound speed error increased up to 2.5 m/s for $\alpha_2 = 10\alpha_W$, because the frequency at which the amplitude spectrum becomes minimum increased. Such error was within 0.2%, which is fairly small compared with the sound speed distributions for tissues.

3. Results and discussion

A specimen of malignant melanoma of the skin was taken. An unstained pathological tissue was fixed with formalin. The specimen was embedded in paraffin, sliced to a thickness of 5–7 μm, and fixed on a slide glass. The specimen was deparaffinized with xylene and ethanol before the ultrasonic measurement.

Table II. Results analyzed by the proposed method for the amplitude and phase spectra in Fig. 3.

α_2/α_W	Analyzed results		
	f_m (MHz)	Thickness (μm)	Sound speed (m/s)
1	55	6.955	1530.1
2	55	6.955	1530.1
10	61	6.281	1532.5

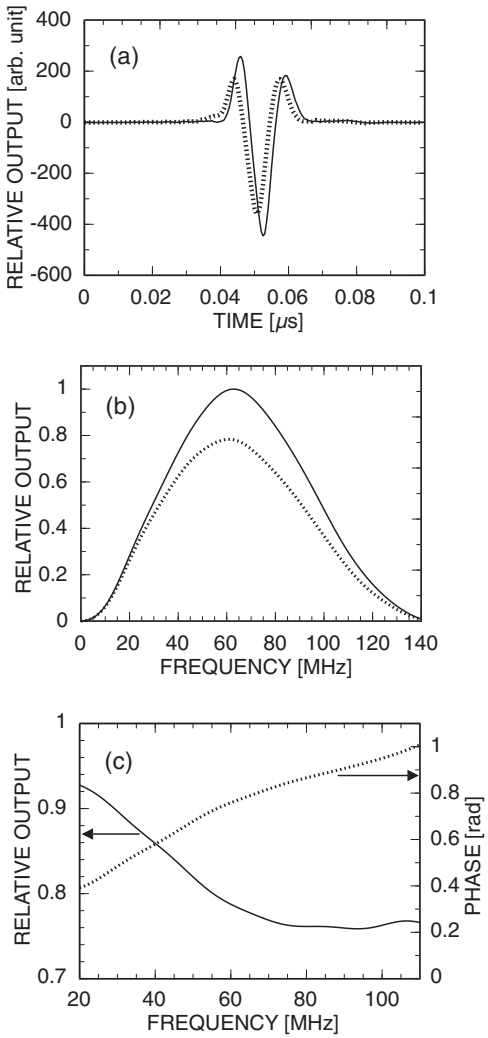

Fig. 5. (a) Reflected signals from a substrate (solid line) and a specimen of malignant melanoma (dotted line) in time domain, (b) frequency spectra of (a) (solid line: substrate, dotted line: specimen), and (c) normalized frequency spectrum (solid line: amplitude, dotted line: phase).

Commercial acoustic microscopy (Honda Electronics AMS-50SI)[8] was used for the measurement using a concave transducer with an ultrasonic transducer of poly(vinylidene fluoride) (PVDF) film, a operating center frequency of 80 MHz, and a focal length of 1.5 mm. Two-dimensional scanning of $2.4 \times 2.4\,mm^2$ was conducted in 8 μm steps. Eight rf signals were measured at each point and averaged. Distilled water was used as the coupler.

The reflected signals from the substrate and specimen are shown in Fig. 5(a). The frequency spectra obtained by fast Fourier transform are shown in Fig. 5(b). The 6 dB bandwidth of the amplitude spectrum reflected from the substrate was 30–100 MHz, and the frequency range was

used for the analysis. The amplitude and phase of the normalized frequency spectrum are shown in Fig. 5(c). The minimum of the amplitude spectrum was observed at 87.2 MHz in Fig. 5(c). The sound speed and thickness of the specimen were obtained as $n = 1$ in Eqs. (6) and (7) from Figs. 4 and 5(c).

The C-mode image of the specimen is shown in Fig. 6. The two-dimensional thickness and sound speed distributions analyzed by the method based on the AR model are shown in Figs. 7(a) and 7(b), respectively. Those along the x-axis direction at $y = 1.5$ mm are shown in Figs. 7(c) and 7(d), respectively. Sound speeds higher than 2,500 m/s and thicknesses larger than 20 μm were observed.

Next, by considering Ref. 5, thicknesses and sound speeds were analyzed using the frequency f_{Min} at which the amplitude spectrum became minimum in the frequency range of 30–100 MHz. The results are shown in Fig. 8. The thicknesses and sound speeds analyzed by the proposed method are shown in Fig. 9. The average, maximum, and minimum values at $y = 1.5$ mm obtained by the proposed method, the method using f_{Min}, and the method based on the AR model are shown in Table III. Variations in sound speeds and thicknesses obtained by the method using f_{Min} and the proposed method were markedly smaller than those obtained by the method based on the AR model.

By comparing the sound speed distribution with the C-mode image, sound speed was observed to increase with decreasing intensity in Fig. 6. This is caused by the increase in acoustic impedance and the decrease in $T_{12} \cdot T_{21}$ in Eq. (3) with higher sound speed.

In the analysis method based on the AR model,[6,7] sound speed and thickness were obtained by estimating the phases of the reflected signals from the normalized frequency spectrum as shown in Fig. 5(c). As one of the factors of large sound speed and thickness errors obtained by the method based on the AR model, it is thought that amplitude of the scattered wave reflected inside the specimen became larger than that of the reflected wave from the specimen surface.

By comparing the results in Figs. 8 and 9, the variation in analyzed thickness obtained by the proposed method was

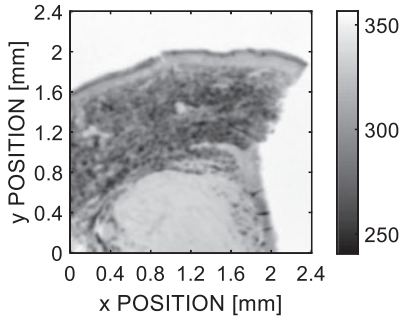

Fig. 6. C-mode image of a specimen of malignant melanoma of skin.

Table III. Thicknesses and sound speeds analyzed by the proposed method in Figs. 9(c) and 9(d), those analyzed by the frequency f_{Min} at which the amplitude spectrum became minimum in Figs. 8(c) and 8(d), and those analyzed by the method based on the AR model in Figs. 7(c) and 7(d).

		Thickness (μm)	Sound speed (m/s)
Proposed method	Ave	5.04	1669
	Max	5.75	1822
	Min	3.86	1505
f_{Min}	Ave	5.16	1671
	Max	6.07	1813
	Min	3.76	1507
AR model	Ave	5.99	1681
	Max	29.3	4069
	Min	−0.01	1473

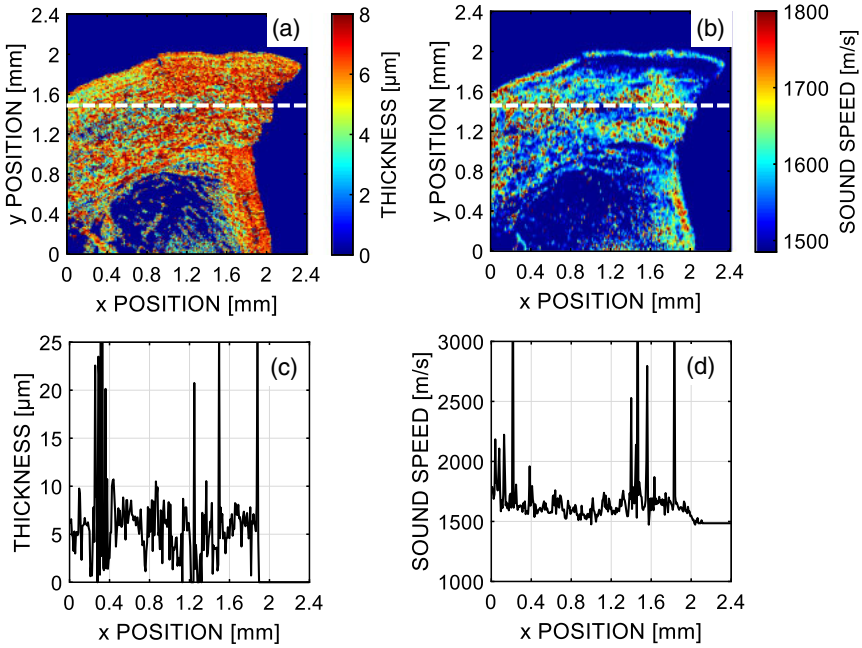

Fig. 7. (Color online) Results analyzed by the method based on the AR model. (a) Thickness distribution, (b) sound speed distribution, (c) thicknesses along $y = 1.5$ mm in (a), and (d) sound speeds along $y = 1.5$ mm in (a).

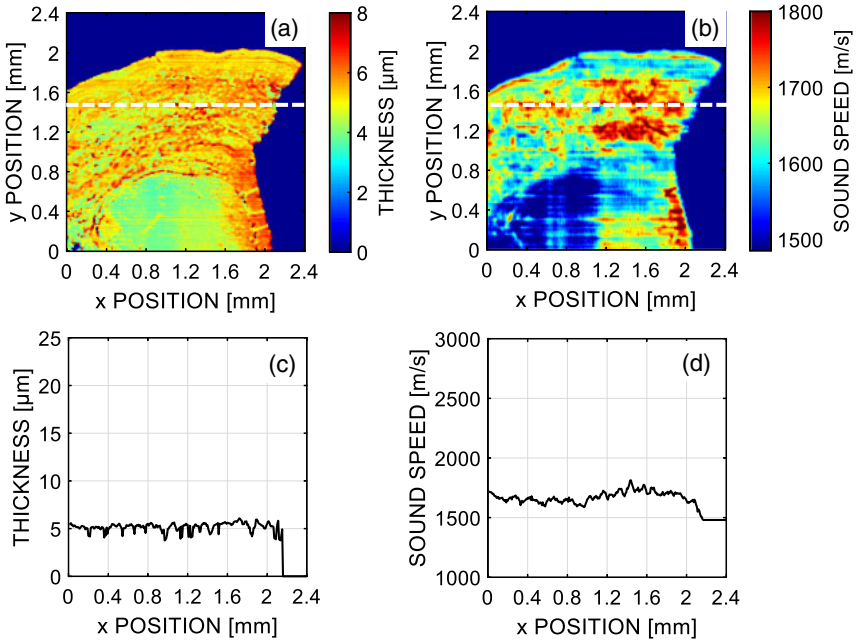

Fig. 8. (Color online) Results analyzed using the frequency f_{Min} at which the amplitude spectrum became minimum in 30–100 MHz range. (a) Thickness distribution, (b) sound speed distribution, (c) thicknesses along $y = 1.5$ mm in (a), and (d) sound speeds along $y = 1.5$ mm in (a).

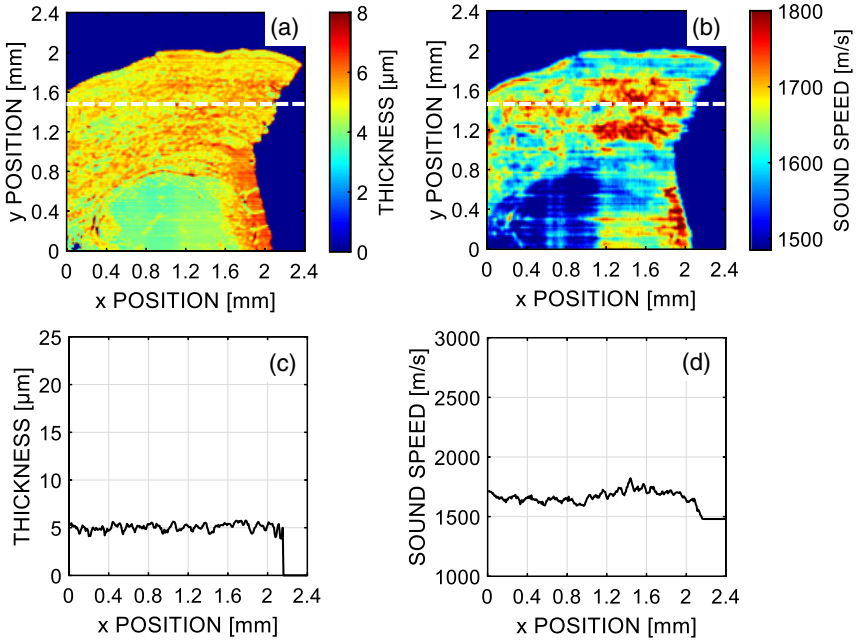

Fig. 9. (Color online) Results analyzed by the proposed method. (a) Thickness distribution, (b) sound speed distribution, (c) thicknesses along $y = 1.5$ mm in (a), and (d) sound speeds along $y = 1.5$ mm in (a).

observed to be smaller than that obtained from f_{Min}, although the analyzed velocities were almost the same. At the point of $(x, y) = (1.1\,\mathrm{mm}, 1.5\,\mathrm{mm})$, d and V_2 were analyzed as 3.94 μm and 1,573 m/s in Fig. 8, and 4.71 μm and 1,578 m/s in Fig. 9, respectively. d obtained from f_{Min} was fairly small. The amplitude spectrum at this point is shown in Fig. 10. f_{m} was determined to be 99.9 and 83.7 MHz by f_{Min} and the proposed method, respectively. The following equations can be obtained from Eqs. (6) and (7):

$$d = \frac{nV_1}{4f_{\mathrm{m}}}\left(1 + \frac{\phi_{\mathrm{m}}}{n\pi}\right), \tag{10}$$

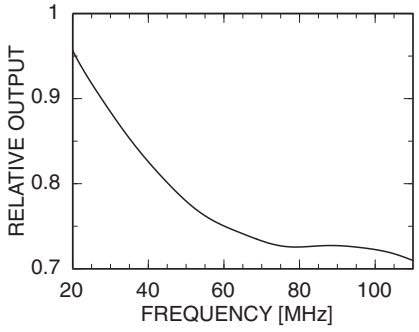

Fig. 10. Amplitude spectrum at $(x, y) = (1.1\,\mathrm{mm}, 1.5\,\mathrm{mm})$.

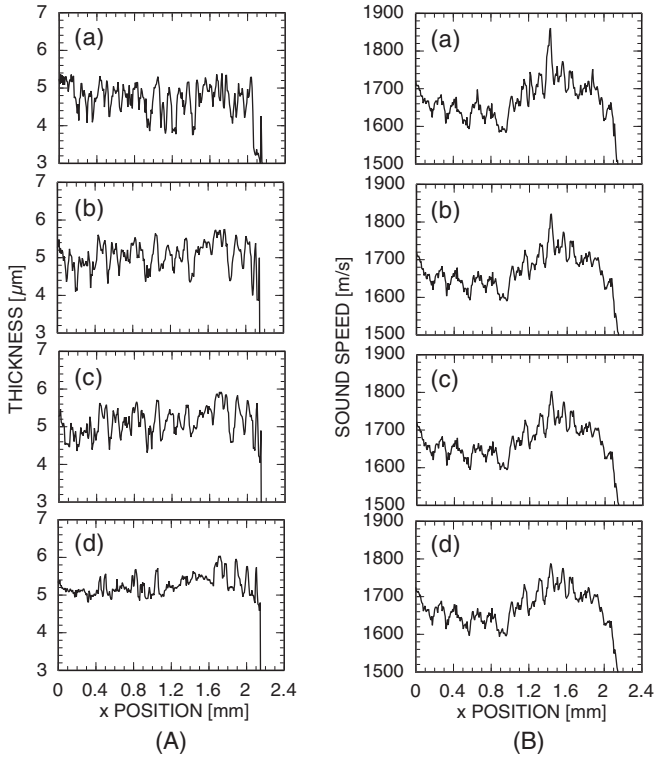

Fig. 11. Thickness (A) and sound speed (B) analyzed by the proposed method at $y = 1.5$ mm by changing the frequency range. (a) 30–120, (b) 30–100, (c) 40–90, and (d) 50–80 MHz.

$$V_2 = V_1\left(1 + \frac{\phi_m}{n\pi}\right). \tag{11}$$

The accuracies of f_m and ϕ_m directly affect that of d from Eq. (10). On the other hand, f_m does not directly affect the accuracy of V_2, but ϕ_m does, as determined from Eq. (11). In Fig. 2, ϕ_m changes from 0.254 to 0.282 rad when the frequency changes from 80 to 88 MHz in the case of $V_2 = 1{,}580$ m/s. With these frequency and phase changes, d and V_2 change by −8.3 and +0.9%, respectively, if $n = 1$ in Eqs. (10) and (11). Therefore, the variation in thickness was reduced by accurately obtaining f_m by the parabolic approximation in the proposed method.

Next, the effect of the frequency range on the analysis in the proposed method was investigated. The frequency ranges of (a) 30–120 MHz, (b) 30–100 MHz, (c) 40–90 MHz, and (d) 50–80 MHz were investigated. The results for $y = 1.5$ mm are shown in Fig. 11. The variations in thickness and sound speed in Fig. 11(a) were slightly larger than those in Figs. 11(b) and 11(c). This is due to the worse signal-to-noise-ratio (SNR) regions in the amplitude spectrum being included in the analysis region, and the decrease in the accuracy of f_m. The minimum thicknesses in Fig. 11(d) were obviously larger than those in Figs. 11(b) and 11(c). This is caused by the limitation of the analysis region. The upper frequency of the analysis was 80 MHz, and the minimum thickness was limited to a value larger than about 5 μm from Fig. 4. From these results, the robustness of the analyzed sound speeds can be improved by selecting an appropriate frequency range for analysis, and that of thicknesses can be improved by accurately obtaining f_m using the parabolic approximation of the amplitude spectrum. Therefore, it is possible to robustly obtain the thickness and sound speed by analyzing the frequency spectrum in the frequency range with good SNR including the minimum or maximum of the amplitude spectrum using the proposed method.

In this experiment, the specimen thickness was controlled to 5–7 μm during specimen preparation. In the present method, the roughly estimated sound speeds and thicknesses are required to investigate the relationship between V_2 and f_m shown in Fig. 4(b). The average sound speeds and thicknesses analyzed by the method based on the AR model were almost the same as those analyzed by the proposed method as shown in Table III. Therefore, those analyzed by the method based on the AR model could be used as rough values to determine the analysis region in the proposed method.

As shown in Fig. 3, the local minimum was not observed in the amplitude spectrum when α_2 was larger than $20\alpha_W$, although intereferences of the amplitude spectrum were observed. If a frequency spectrum is measured more than a cycle, the low-frequency component of the amplitude spectrum can be obtained by the linear approximation, and only the interference component can be extracted by subtracting it from the amplitude spectrum. Thereafter, the analysis using the proposed method would be conducted.

4. Conclusions

In this paper, a robust analysis method for the acoustic properties of biological specimens measured by acoustic microscopy is proposed. Average acoustic properties can be obtained by the proposed method considering the operating frequency range of the ultrasonic device, even if there are unwanted ripples on the amplitude spectrum because of the low SNR or existence of scattered waves. The proposed method is useful for the analysis of the acoustic properties of biological tissues or cells.

1) A. Korpel, L. W. Kessler, and P. R. Palermo, Nature **232**, 110 (1971).
2) R. A. Lemons and C. F. Quate, Proc. IEEE Ultrasonics Symp., 1973, p. 18.
3) R. A. Lemons and C. F. Quate, Science **188**, 905 (1975).
4) G. A. D. Briggs, J. Wang, and R. Gundle, J. Microsc. **172**, 3 (1993).
5) N. Hozumi, R. Yamashita, C.-K. Lee, M. Nagao, K. Kobayashi, Y. Saijo, M. Tanaka, N. Tanaka, and S. Ohtsuki, Acoust. Sci. Technol. **24**, 386 (2003).
6) N. Tanaka, K. Kobayashi, N. Hozumi, Y. Saijo, M. Tanaka, and S. Ohtsuki, Rep. Spring Meet. Acoustical Society of Japan, 2003, p. 1345 [in Japanese].
7) N. Tanaka, K. Kobayashi, N. Hozumi, Y. Saijo, M. Tanaka, and S. Ohtsuki, Tech. Rep. IEICE **105**, 21 (2005) [in Japanese].
8) K. Kobayashi, N. Hozumi, Y. Saijo, and S. Ohtsuki, J. Acoust. Soc. Jpn. **62**, 148 (2006).
9) J. A. Hildebrand and D. Rugar, J. Microsc. **134**, 245 (1984).
10) H. Lüers, K. Hillmann, J. Litniewski, and J. Bereiter-Hahn, Cell Biophys. **18**, 279 (1991).
11) A. Kinoshita, S. Senda, K. Mizushige, H. Masugata, S. Sakamoto, H. Kiyomoto, and H. Matsuo, Ultrasound Med. Biol. **24**, 1397 (1998).
12) T. Kundu, J. Bereiter-Hahn, and I. Karl, Biophys. J. **78**, 2270 (2000).
13) Y. Saijo, M. Tanaka, H. Okawai, and F. Dunn, Ultrasound Med. Biol. **17**, 709 (1991).
14) Y. Saijo, M. Tanaka, H. Okawai, H. Sasaki, S. Nitta, and F. Dunn, Ultrasound Med. Biol. **23**, 77 (1997).
15) R. M. Lemor, E. C. Weiss, G. Pilarczyk, and P. V. Zinin, Proc. IEEE Int. Ultrasonics, Ferroelectr. Freq. Control, 2004, p. 622.
16) P. V. Zinin, P. Anastasiadis, E. C. Weiss, and R. M. Lemor, Proc. IEEE Int. Ultrasonics Symp., 2007, p. 813.
17) E. C. Weiss, P. Anastasiadis, G. Pilarczyk, R. M. Lemor, and P. V. Zinin, IEEE Trans. Ultrason. Ferroelectr. Freq. Control **54**, 2257 (2007).
18) E. M. Strohm and M. C. Kolios, Proc. 31st Annu. Int. Conf. IEEE Engineering in Medicine and Biology Society, 2009, p. 6042.

19) E. M. Strohm, G. J. Czarnota, and M. C. Kolios, IEEE Trans. Ultrason. Ferroelectr. Freq. Control **57**, 2293 (2010).
20) Y. Saijo, N. Hozumi, C. Lee, M. Nagao, K. Kobayashi, N. Okada, N. Tanaka, E. S. Filho, H. Sasaki, M. Tanaka, and T. Yambe, Ultrasonics **44**, e51 (2006).
21) Y. Saijo, E. S. Filho, H. Sasaki, T. Yambe, M. Tanaka, N. Hozumi, K. Kobayashi, and N. Okada, IEEE Trans. Ultrason. Ferroelectr. Freq. Control **54**, 1571 (2007).
22) Y. Saijo, Imaging Med. **1**, 47 (2009).
23) M. Arakawa, J. Shikama, K. Yoshida, R. Nagaoka, K. Kobayashi, and Y. Saijo, IEEE Trans. Ultrason. Ferroelectr. Freq. Control **62**, 1615 (2015).
24) K. Miura, H. Nasu, and S. Yamamoto, Sci. Rep. **3**, 1255 (2013).
25) K. Miura and S. Yamamoto, Sci. Rep. **5**, 15243 (2015).
26) K. Miura, Y. Egawa, T. Moriki, H. Mineta, H. Harada, S. Baba, and S. Yamamoto, Pathol. Int. **65**, 355 (2015).
27) K. Miura and S. Yamamoto, Lab. Invest. **92**, 1760 (2012).
28) T. Yamaoka, T. Yamaguchi, M. Sekine, S. Zenbutsu, H. Matsubara, and H. Hayashi, Jpn. J. Appl. Phys. **52**, 07HF20 (2013).
29) M. Omura, K. Yoshida, M. Kohta, T. Kubo, T. Ishiguro, K. Kobayashi, N. Hozumi, and T. Yamguchi, Jpn. J. Appl. Phys. **55**, 07KF14 (2016).
30) D. Rohrbach, K. Ito, H. O. Lloyd, R. H. Silverman, K. Yoshida, T. Yamaguchi, and J. Mamou, Ultrason. Imaging **39**, 313 (2017).
31) D. Rohrbach, A. Jakob, H. O. Lloyd, S. H. Tretbar, R. H. Silverman, and J. Mamou, IEEE Trans. Biomed. Eng. **64**, 715 (2017).